Author(s): Laitinen, Antti & Kumar, Manohar & Oksanen, Mika & Placais, Bernard & Virtanen, Pauli & Hakonen, Pertti J.

Title: Coupling between electrons and optical phonons in suspended bilayer graphene

Year: 2015

Version: Final published version

**Please cite the original version:**

Laitinen, Antti & Kumar, Manohar & Oksanen, Mika & Placais, Bernard & Virtanen, Pauli & Hakonen, Pertti J. 2015. Coupling between electrons and optical phonons in suspended bilayer graphene. Physical Review B. Volume 91, Issue 12. 121414/1-5. DOI: 10.1103/physrevb.91.121414

PHYSICAL REVIEW B **91**, 121414(R) (2015)

# Coupling between electrons and optical phonons in suspended bilayer graphene

Antti Laitinen,[1] Manohar Kumar,[1] Mika Oksanen,[1] Bernard Plaçais,[1,2] Pauli Virtanen,[1] and Pertti Hakonen[1]

[1]*Low Temperature Laboratory, Department of Applied Physics, Aalto University, 00076 Aalto, Finland*

[2]*Laboratoire Pierre Aigrain, Ecole Normale Supérieure, CNRS (UMR8551), Université Pierre et Marie Curie, Université Paris Diderot, 75231 Paris, France*

(Received 27 August 2014; revised manuscript received 2 March 2015; published 27 March 2015)

Using electrical transport experiments and shot noise thermometry, we investigate electron-phonon heat transfer rate in a suspended bilayer graphene. Contrary to monolayer graphene with heat flow via three-body supercollision scattering, we find that regular electron–optical-phonon scattering in bilayer graphene provides the dominant scattering process at electron energies $\gtrsim$0.15 eV. We determine the strength of these intrinsic heat flow processes of bilayer graphene and find good agreement with theoretical estimates when both zone edge and zone center optical phonons are taken into account.

DOI: 10.1103/PhysRevB.91.121414 PACS number(s): 81.05.ue

Electron-phonon coupling has been investigated extensively in monolayer graphene (MLG), both theoretically [1–6] and empirically in quantum transport experiments [7–10]. The weak coupling between acoustic phonons and electrons limits electronic cooling, and as a result extrinsic processes ("supercollisions") take over in typical samples [8,11], even in suspended ones [10]. In supercollisions, the restrictions in energy transfer by single acoustic phonon scattering [6] are circumvented via three-body collisions, where disorder facilitates for the participation of phonons with a larger momentum in the scattering process. Understanding the scattering processes in monolayer and bilayer graphene is important for designing high-quality graphene transistors in which the mobility at large bias will be limited by the scattering from optical phonons in the absence of extrinsic processes.

Except for the small energies [12], the electronic band structure of bilayer graphene (BLG) is quite different from the monolayer (MLG): instead of massless Dirac fermions, the bilayer has massive particles as charge carriers. This results in a larger density of states (DOS) of the electrons: the ratio of DOS at energy $E$ is given by $\gamma_1/|E|$, where $\gamma_1 \approx 0.4$ eV corresponds to hopping between the two layers in bilayer graphene [13]; the difference can be further amplified by velocity renormalization effects in MLG [14]. In addition to increasing the general electron-phonon heat flow in a bilayer as compared to a monolayer, these differences also turn out to contribute toward increasing the relative importance of scattering from optical phonons in bilayer graphene.

In this work, we have employed shot noise thermometry and conductance measurements to determine the electron-phonon coupling in high-quality, suspended bilayer graphene at large bias voltages. We demonstrate that in bilayers we can reach the intrinsic behavior at high bias, and that the electron-phonon scattering is governed by optical phonons. At bias voltages corresponding to electronic temperatures >300 K, we find strong enhancement of the electron-phonon coupling due to optical phonons which results in a typical thermal-activation type of growth of the heat flow (cf. Fig. 1). The magnitude of the power flow can be well accounted for by the existing theories for a bilayer when long wave length longitudinal (LO) and transverse (TO) optical modes around the zone center (ZC, $\Gamma$ point) are taken into account with additional contributions from zone edge modes (ZE, $K$ point). In the regime of optical-phonon scattering, only a weak dependence on chemical potential is observed, consistent with theory [3,4].

Several different phonon scattering processes are expected to contribute to the transfer of heat from the charge carriers, i.e., electrons or holes, to the lattice in BLG. First, the estimate for the effect of collisions with acoustic phonons can be characterized by a power law $P = \Sigma(T_e^\delta - T_{\rm ph}^\delta)$, where $T_e$ is the electron temperature, $T_{\rm ph}$ the phonon temperature, $\Sigma$ the coupling constant, and $\delta$ a characteristic exponent [16]. The maximum change of momentum at the Fermi level is twice the Fermi momentum $2k_F$, which corresponds to phonon energy $\hbar\omega_{2k_F}$. This energy defines a characteristic temperature, the Bloch-Grüneisen temperature, $k_B T_{\rm BG} = \hbar\omega_{2k_F} \approx 18\,K \times \sqrt{n/10^{11}\,{\rm cm}^{-2}}$, above which only a fraction of acoustic phonons are available for scattering with electrons in the thermal window. Our bilayer graphene experiments have been conducted near the Dirac point at charge densities $n < (0.1-3.4)\times 10^{11}{\rm cm}^{-2}$, which corresponds to $T_{\rm BG} < 34$ K for longitudinal acoustic phonons. Using the Kapitza resistance from Ref. [17], we find that all our high-bias results have been measured in the regime of $T > T_{\rm BG}$, where the scattering of electrons from acoustic phonons leads to $\delta = 1$ or $\delta = 2$, depending on whether $k_B T_e << \mu$ or $k_B T_e > \mu$, respectively [4]. Here $\mu$ denotes the chemical potential.

The power density to the zone center (ZC) longitudinal and transverse optical modes in BLG, which have energies $\Omega_{\rm ZC} \approx 0.2$ eV, can be estimated as [4]

$$P_{e\text{-op}}^{\rm (ZC)} = \frac{18A\Omega_{\rm ZC}^3(\gamma_0')^2\hbar}{\pi(\hbar v_0)^4\rho}\frac{\gamma_1}{\Omega_{\rm ZC}}[n_e(\Omega_{\rm ZC}) - n_{\rm op}(\Omega_{\rm ZC})]\mathcal{G}(\mu,T_e). \tag{1}$$

Here, $A$ is the sheet area, $\gamma_0' = 42$ eV/nm [18], $\rho = 4M_C N/A$, $v_0 \approx 10^6$ m/s, and $n_e(\Omega_{\rm ZC})$ and $n_{\rm op}(\Omega_{\rm ZC})$ are Bose distribution functions evaluated at temperatures $T_e$ and $T_{\rm ph}$. Finally,

$$\mathcal{G}(\mu,T_e) = \int_{-\infty}^{\infty}\frac{1}{4}(|x|+|x-1|)[f(\Omega_{\rm ZC}(x-1)) - f(\Omega_{\rm ZC}x)]\,dx \tag{2}$$

describes the dependence on the chemical potential. We assume that the coupling between optical and acoustic phonons is not limiting the energy flow [19,20], and consider the optical-phonon temperature $T_{\rm ph}$ as a constant.

 

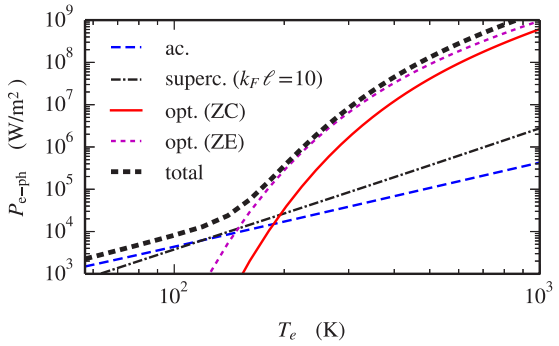


FIG. 1. (Color online) Theoretical estimates for the power density from electrons to phonons in bilayer graphene as a function of electronic temperature $T_e$ (for $n = 10^{11}\,\mathrm{cm}^{-2}$ and $T_{\mathrm{ph}} = 0$), due to different phonon scattering processes. Acoustic and optical ZC phonon results are from Eqs. (21) and (30) in Ref. [4], assuming gauge potential $D_2 = \hbar v_F \beta/(2a) \approx 7\,\mathrm{eV}$ and screened deformation potential [15] $D_1(q = k_F) = 0.6\,\mathrm{eV}$. Supercollision and ZE estimates are as from Eqs. (3) and (4) below.

Intervalley scattering by zone edge (ZE) optical phonons also contributes to the heat current. In MLG, the ZE point optical modes dominate over ZC phonons in resistance [21,22]. The results of Ref. [21] indicate $\sum\langle M^2_{\mathrm{ZE},j}\rangle / \sum\langle M^2_{\mathrm{ZC},j}\rangle = \Omega_{\mathrm{ZC}}/\Omega_{\mathrm{ZE}} \approx 1.3$ for the ratio of the angle-averaged squared matrix elements, which are relevant for the heat current. The corresponding power density is obtained by substituting $\Omega_{\mathrm{ZC}}$ with $\Omega_{\mathrm{ZE}}$ in Eqs. (1) and (2).

The total heat flow by optical phonons is the sum of these two contributions: $P_{e\text{-op}} = P^{(\mathrm{ZE})}_{e\text{-op}} + P^{(\mathrm{ZC})}_{e\text{-op}}$. Unfortunately, we are not aware of microscopic results for electron-ZE-phonon coupling in BLG. We can, however, obtain a rough estimate by assuming that the ratio of matrix elements is similar in BLG to that in MLG, in which case the ZE contribution becomes

$$P^{(\mathrm{ZE})}_{e\text{-op}} \approx \frac{\Omega_{\mathrm{ZC}}}{\Omega_{\mathrm{ZE}}} \times P_{e\text{-op}}|_{\Omega=\Omega_{\mathrm{ZE}}}\,. \tag{3}$$

At temperatures $T = 300$–$1000\,\mathrm{K}$, the two contributions are of the same order of magnitude, $P^{(\mathrm{ZE})}_{e\text{-op}} = 4P^{(\mathrm{ZC})}_{e\text{-op}}\mathrm{to}1.5P^{(\mathrm{ZC})}_{e\text{-op}}$.

Finally, the effect of acoustic phonon supercollisions in BLG can be estimated similarly as derived for MLG in Ref. [11]. Within the quadratic dispersion approximation and a screened (Thomas-Fermi) BLG electron-phonon interaction model [15], the power density becomes

$$P_{e\text{-ph}} \approx \frac{9.62\tilde{g}^2\nu_1^2}{2\hbar(k_F\ell)_{\mathrm{MLG}}} k_B^3\left(T_e^3 - T_{\mathrm{ph}}^3\right), \quad \tilde{g}^2 = \frac{\frac{D_1^2}{4\alpha^2} + D_2^2}{2\rho s_L^2}\,, \tag{4}$$

for $T > T_{\mathrm{BG}}$. Here, $\nu_1 = \gamma_1/(4\pi\hbar^2 v_0^2)$ is the density of states (DOS) per valley per spin in bilayer graphene, $D_1 \approx 20$–$50\,\mathrm{eV}$ is the bare deformation potential coupling, $D_2 = \frac{\beta\hbar v_0}{2a} \approx 7\,\mathrm{eV}$ the gauge potential coupling [15], $s_L \approx 2.1 \times 10^4\,\mathrm{m/s}$ the longitudinal acoustic phonon velocity, and $\alpha = e^2/(4\pi\epsilon_0\hbar v_0) \approx 2$. Moreover, $(k_F\ell)_{\mathrm{MLG}} = 2\hbar^2 v_0^2/(u^2 n_0)$ is a dimensionless measure of short-range impurity concentration $n_0$ with $\delta$ function potential of strength $u$.

Figure 1 summarizes the expected magnitudes of the different contributions: the optical phonons are expected to dominate the heat flow at large temperatures. Note that the bilayer electron–optical-phonon coupling is around two orders of magnitude larger than in MLG near the Dirac point, when the renormalization of the Fermi velocity in the suspended monolayer [23] is taken into account.

TABLE I. Parameters for our two bilayer graphene samples denoted by S1 and S2. The length and width are given in $\mu$m by $L$ and $W$, respectively. $R_0$ is the maximum resistance at the Dirac point which corresponds to minimum conductivity $\sigma_m$ as multiples of $\sigma_0 = \frac{4e^2}{\pi h}$, while $R_C$ is an estimate for the high-frequency contact resistance. The last column indicates the field effect mobility (in cm$^2$/Vs) deduced from the gate sweeps. Sample S1 is an HF-underetched device on silicon dioxide whereas S2 was fabricated on a lift-off resist.

| S # | $L$ | $W$ | $R_0$ | $\sigma_m/\sigma_0$ | $R_C$ | $V_D$ | $\mu_f$ |
|---|---|---|---|---|---|---|---|
| S1 | 0.43 | 0.51 | 5.8 kΩ | 3.0 | 100 Ω | −0.3 V | 14000 |
| S2 | 0.83 | 3.2 | 1.5 kΩ | 3.6 | 30 Ω | 0.6 V | 6200 |

The studied bilayer samples are listed in Table I: their length varied over $L = 0.4$–$0.8\,\mu\mathrm{m}$ and the width $W = 0.5$–$3.2\,\mu\mathrm{m}$. The samples studied here are exfoliated graphene suspended on $SiO_2$ (S1) and lift-off resist (S2). Leads were patterned using electron-beam lithography. Raman spectroscopy was employed to verify that the sample was a bilayer graphene sheet. Prior to measurements, all samples were cleaned by current annealing using a current of $\sim 1\mathrm{mA}/\mu\mathrm{m}$ in cryogenic vacuum. The resulting high-quality samples were nearly neutral, with the charge neutrality (Dirac) point located at $|V_g^D| < 0.6\,\mathrm{V}$. The gate capacitance was determined from the parallel plate capacitor model: $C_g = 5.2$–$4.7\,\frac{\mathrm{nF}}{\mathrm{cm}^2}$ for different samples. A SEM image of sample S2 is shown in Fig. 2. The graphene sheet has a wavy structure, which indicates the presence of tensile stress at room temperature. Strain may be the reason why no clear signs of flexural modes [15] were observed in the $I/V$ measurements on our bilayer samples (see Supplemental Material [24] with Refs. [25–34]).

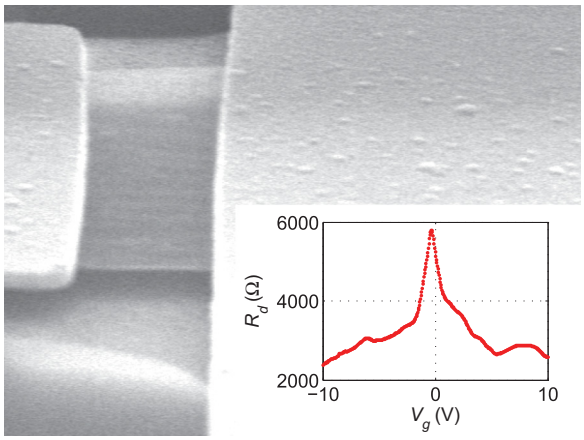


FIG. 2. (Color online) Scanning electron micrograph of our suspended graphene sample S2. The metallic leads for contacting graphene were made of Cr/Au. The inset displays zero-bias resistance vs $V_g$ for S1.

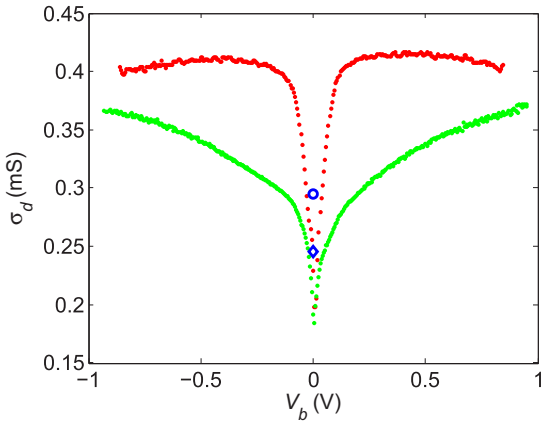


FIG. 3. (Color online) (a) Differential conductivity $\sigma_d$ vs bias voltage $V_b$ near the Dirac point at $V_g = +0$ V for S1 (red, upper) and S2 (green, lower). The theoretical result for bilayer $24\frac{e^2}{\pi h}$ [35] is marked by ○; the experimental result by Mayorov *et al.* [36] on suspended bilayer is denoted by ◊.

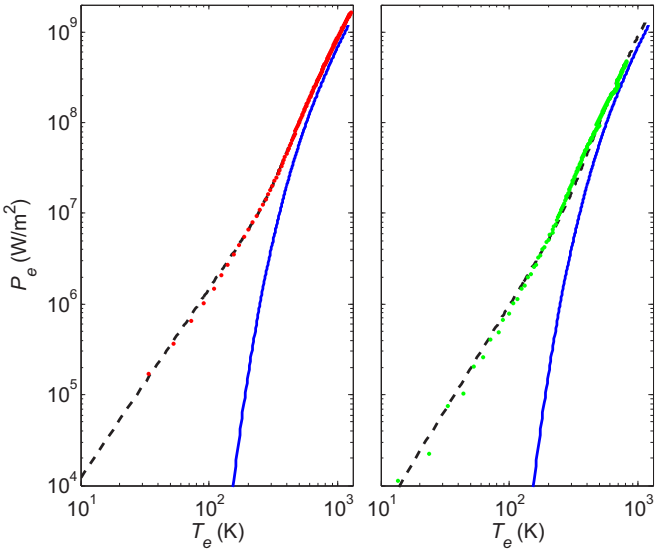


FIG. 4. (Color online) Joule heating in bilayer graphene $P_e$ as a function of electron temperature $T_e = Fe|V|/2k_B$ near the Dirac point at $n = 10^{10}\ \frac{1}{\mathrm{cm}^2}$. The left (sample S1) and the right (sample S2) frames represent measured data in circles while the theoretical behavior ($P_{\mathrm{WF}} + P_{e\text{-op}}^{(\mathrm{ZC})} + P_{e\text{-op}}^{(\mathrm{ZE})}$) is expressed using dashed black curves; the blue solid curves denote the contributions of optical phonons ($P_{e\text{-op}}^{(\mathrm{ZC})} + P_{e\text{-op}}^{(\mathrm{ZE})}$).

The inset in Fig. 2 displays the variation of zero-bias resistance $R_0 = dV/dI_{|V=0}$ vs gate voltage $V_g$ over chemical potentials ranging ±12 meV across the Dirac point. The gate sweep indicates that minimum charge density is around $1 \times 10^{10}$ cm$^{-2}$ in our bilayer samples. The initial slope of $G_0(n) = 1/R_0$ was employed to determine the field effect mobility which reached $\mu_f = 1.4 \times 10^4$ cm$^2$/Vs in sample S1.

Figure 3 displays differential conductance vs bias voltage for the samples. Initially, there is a strong increase in conductance with respect to bias voltage, which has been interpreted as a self-heating of the bilayer [37]. The increase is cut off at bias values close to the optical-phonon energy [38]. On the other hand, flexural phonons were found to play a role in a monolayer by facilitating supercollisions at high bias; their presence was observed in the total resistance as a temperature-dependent contribution which behaved as $V/I \propto T^2$ [10]. In the Supplemental Material [24] we show that the integrated data of Fig. 3 yields $V/I \propto T_e$ and no indications of flexural modes are observed. The most likely explanation for this is that strain changes the dispersion relation of flexural modes from quadratic to linear, making the $T^2$ component negligible. The measured minimum conductivity is around $\frac{13e^2}{\pi h}$ and quite close to the results of Mayorov *et al.* [36] on similar suspended bilayer samples.

Besides current voltage characteristics, the zero frequency shot noise (600–900 MHz) and its first harmonic were measured to deduce the electronic temperature of BLG under high bias. The basic argument for shot noise thermometry are found in Refs. [20,39] and its recent applications in graphene are found in Refs. [7,10]. Noise spectral density of a Poissonian process is given by $S_p = 2q\langle I\rangle$, where $\langle I\rangle$ is the average current. The Fano factor defines the noise level $S_I$ with respect to the Poissonian noise, $F = S_I/S_p$ [40]. In addition to gate voltage, the Fano factor depends on the bias voltage $V$ (see the Supplemental Material [24]). When the bias voltage is increased, enhanced electron-electron interactions try to bring the system towards the so-called hot electron regime with $F = \sqrt{3}/4$, whereas inelastic scattering causes a tendency towards classical behavior without any shot noise.

Shot noise thermometry was used to determine the temperature of electrons in graphene under Joule heating. The temperature $T_e = \frac{Fe|V|}{2k_B}$ is an average over spatial distribution of temperature which, in the regime of strong electron-phonon scattering, yields rather accurately the actual electronic temperature in the center of the sample; the Fano factor for noise thermometry was adjusted for the contact resistance as in Ref. [10]. Our experiments were performed on a pulse-tube-based dilution refrigerator operated around 0.5 K. For experimental details, we refer to Refs. [41,42].

The Joule heating power to graphene electrons equals $P_e = VI - R_C I^2$ where $R_C$ denotes the effective high-frequency contact resistance [43,44] (see Table I). Figure 4 displays $P_e$ vs $T_e$ measured up to $10^9$W/m$^2$. Due to weak electron-phonon coupling at low bias, the electronic heat conduction governed by the Wiedemann-Franz law dominates other thermal processes. The power $P_{\mathrm{WF}} = G\frac{\pi^2}{3}\frac{k_B^2}{e^2}(T_e^2 - T_B^2)$ is carried to the leads at temperature $T_B$. On the other hand, at large bias, x electron-phonon coupling is strong and hence heat transport to phonons ($P_{e\text{-ph}}$) dominates. Due to the short length of the samples investigated here, $P_{e\text{-ph}}$ is seen to dominate the measured $P_e(T_e)$ first above 200–300 K. For acoustic phonons, temperature dependence of $\propto T^2$ is expected in bilayers ($\delta = 2$), but the theoretical estimates (see Fig. 1) indicate power flows that are well below the observed levels unless the deformation potential is made exceedingly large. Above 300 K, the results indicate an onset of an additional relaxation channel which initially leads to steeper $T$ dependence, but whose growth rate becomes slightly weaker with growing temperature. This onset behavior is similar to that calculated for optical

phonons in Fig. 1 (see also the fits in Fig. 4). As the data sets coincide at high temperatures, the coupling we measure is truly an intrinsic property of bilayer graphene; in the Wiedemann-Franz regime at low temperatures, the behaviors at different lengths deviate from each other because of scaling as $1/L^2$.

In the high-$T$ regime where phonon scattering dominates the electronic heat diffusion, we find quite weak dependence of $P_e$ on chemical potential (see Fig. S6 of the Supplemental Material [24]). In the measured range ($-12 < \mu < 12$ meV), all the variation of the absorbed heat flux $P_e$ at constant $T_e$ can be accounted for by a change in $P_{\mathrm{WF}}$ due to the variation of $R(V_g)$. The independence of electron-phonon coupling on $\mu$ is in agreement with optical or acoustic phonons in BLG with $T_{\mathrm{ac}} > T_{\mathrm{BG}}$ and $k_B T_e >> \mu$. The observed temperature dependence of the coupling, however, rules out the latter possibility, because in that regime $P_{e\text{-op}} \propto T_e^2 - T_{\mathrm{ph}}^2$ [4]. We note that the weak gate dependence of $P_{e\text{-ph}}$ does not rule out supercollisions since they predict $\mu$-independent behavior due to constant density of states in the bilayer. The best check for supercollision scattering is to scrutinize $P_e/T_e^3$, which shows no plateau and so rules out the supercollision processes [7] (see Fig. S5 in the Supplemental Material [24]).

In Fig. 4, we compare our data to the sum $P_{\mathrm{WF}} + P_{e\text{-op}}^{(\mathrm{ZC})} + P_{e\text{-op}}^{(\mathrm{ZE})}$ using parameters specified below Eq. (1), except that $\gamma_0'$ is left as a fit parameter. In our experiments at weak doping, the best fit is obtained with $\gamma_0' \approx 37$ eV/nm, as illustrated by the fits in Fig. 4. This is slightly smaller than the value $\gamma_0' = 42$ eV/nm obtained in Ref. [18] and $\gamma_0' = 47.5$ eV/nm found in Ref. [21]. Using $\gamma_0' = 42$ eV/nm, our results would imply nearly equal contributions from ZC and ZE phonons to heat current. Altogether, the optical phonons together with the Wiedemann-Franz law give a very good agreement between experiment and theory as indicated by the fits in Fig. 4 (see also Fig. S5 in the Supplemental Material [24]).

Compared with monolayer experiments [8,10], our results on the electron-phonon coupling are rather close in magnitude in the degenerate limit ($\mu > k_B T$) at high bias. At small chemical potentials, the constant density of states in a bilayer implies stronger phonon scattering in the bilayer. According to Ref. [4], optical-phonon heat flow is larger by a factor of 3 in the bilayer than in the monolayer, and this difference grows further with Fermi level renormalization near the Dirac point. Furthermore, the rigidity of the bilayer is larger than for a monolayer [15] which, on its part, diminishes the strength of the flexural phonon supercollisions in bilayers. These issues account for the fact that only in bilayers are we able to observe intrinsic scattering by optical phonons, while flexural-mode-induced supercollisions appear in suspended monolayers.

In summary, our experiments indicate a strong difference between electron-phonon heat relaxation at high bias in suspended monolayer and bilayer graphene. Using electrical transport experiments and shot noise thermometry, we find that electron–optical-phonon scattering dominates in bilayer graphene at electronic temperatures of 300–1000 K, induced by bias voltages comparable to optical-phonon energies. The strength of the scattering follows theoretical expectations with a specific thermal activation behavior, and indicates the presence of intervalley electron scattering by zone edge and zone center optical phonons. This electron-phonon coupling is found to be independent of the gate-induced chemical potential at $|\mu| < 12$ meV, which is in accordance with the theory for optical-phonon scattering.

We acknowledge fruitful discussions with J. Viljas, T. Heikkilä, M. Tomi, and F. Mauri. Our work was supported by the Academy of Finland (Contracts No. 135908 and No. 250280, LTQ CoE). The research leading to these results has received funding from the European Union Seventh Framework Programme under Grant Agreement No. 604391 Graphene Flagship, and the work benefited from the use of the Aalto University Low Temperature Laboratory infrastructure. M.O. is grateful to Väisälä Foundation of the Finnish Academy of Science and Letters for a scholarship.

[1] S. S. Kubakaddi, Phys. Rev. B **79**, 075417 (2009).
[2] W.-K. Tse and S. Das Sarma, Phys. Rev. B **79**, 235406 (2009).
[3] R. Bistritzer and A. H. MacDonald, Phys. Rev. Lett. **102**, 206410 (2009).
[4] J. K. Viljas and T. T. Heikkilä, Phys. Rev. B **81**, 245404 (2010).
[5] H. Suzuura and T. Ando, Phys. Rev. B **65**, 235412 (2002).
[6] M. I. Katsnelson, *Graphene: Carbon in Two Dimensions*, 1st ed. (Cambridge University, New York, 2012).
[7] A. C. Betz, S. H. Jhang, E. Pallecchi, R. Ferreira, G. Fève, J.-M. Berroir, and B. Plaçais, Nat. Phys. **9**, 109 (2012).
[8] A. C. Betz, F. Vialla, D. Brunel, C. Voisin, M. Picher, A. Cavanna, A. Madouri, G. Fève, J.-M. Berroir, B. Plaçais, and E. Pallecchi, Phys. Rev. Lett. **109**, 056805 (2012).
[9] J. Yan, M.-H. Kim, J. A. Elle, A. B. Sushkov, G. S. Jenkins, H. M. Milchberg, M. S. Fuhrer, and H. D. Drew, Nat. Nanotech. **7**, 472 (2012).
[10] A. Laitinen, M. Oksanen, A. Fay, D. Cox, M. Tomi, P. Virtanen, and P. Hakonen, Nano Lett. **14**, 3009 (2014).
[11] J. C. W. Song, M. Y. Reizer, and L. S. Levitov, Phys. Rev. Lett. **109**, 106602 (2012).
[12] E. McCann and V. I. Falko, Phys. Rev. Lett. **96**, 086805 (2006).
[13] A. Misu, E. E. Mendez, and M. S. Dresselhaus, J. Phys. Soc. Jpn. **47**, 199 (1979).
[14] V. N. Kotov, B. Uchoa, V. M. Pereira, F. Guinea, and A. H. Castro Neto, Rev. Mod. Phys. **84**, 1067 (2012).
[15] H. Ochoa, E. V. Castro, M. I. Katsnelson, and F. Guinea, Phys. Rev. B **83**, 235416 (2011).
[16] F. Giazotto, T. T. Heikkilä, A. Luukanen, A. M. Savin, and J. P. Pekola, Rev. Mod. Phys. **78**, 217 (2006).
[17] X. Song, M. Oksanen, J. Li, P. J. Hakonen, and M. A. Sillanpää, Phys. Rev. Lett. **113**, 027404 (2014).
[18] J. Yan, Y. Zhang, P. Kim, and A. Pinczuk, Phys. Rev. Lett. **98**, 166802 (2007).
[19] N. Bonini, M. Lazzeri, N. Marzari, and F. Mauri, Phys. Rev. Lett. **99**, 176802 (2007).

[20] F. Wu, P. Virtanen, S. Andresen, B. Plaçais, and P. J. Hakonen, Appl. Phys. Lett. **97**, 262115 (2010).

[21] C.-H. Park, N. Bonini, T. Sohier, G. Samsonidze, B. Kozinsky, M. Calandra, F. Mauri, and N. Marzari, Nano Lett. **14**, 1113 (2014).

[22] T. Fang, A. Konar, H. Xing, and D. Jena, Phys. Rev. B **84**, 125450 (2011).

[23] D. C. Elias, R. V. Gorbachev, A. S. Mayorov, S. V. Morozov, A. A. Zhukov, P. Blake, L. A. Ponomarenko, I. V. Grigorieva, K. S. Novoselov, F. Guinea, and A. K. Geim, Nat. Phys. **7**, 701 (2011).

[24] See Supplemental Material at http://link.aps.org/supplemental/10.1103/PhysRevB.91.121414 for extended presentation of the experimental data and sample characterization.

[25] K. I. Bolotin, K. J. Sikes, J. Hone, H. L. Stormer, and P. Kim, Phys. Rev. Lett. **101**, 096802 (2008).

[26] N. Tombros, A. Veligura, J. Junesch, J. Jasper van den Berg, P. J. Zomer, M. Wojtaszek, I. J. Vera Marun, H. T. Jonkman, and B. J. van Wees, J. Appl. Phys. **109**, 093702 (2011).

[27] A. H. Steinbach, J. M. Martinis, and M. H. Devoret, Phys. Rev. Lett. **76**, 3806 (1996).

[28] K. E. Nagaev, Phys. Rev. B **52**, 4740 (1995).

[29] J. Sarkar, Microwave experiments and noise in mesoscopic devices, Ph.D. thesis, Aalto University, 2015 (unpublished).

[30] C.-H. Park, F. Giustino, M. L. Cohen, and S. G. Louie, Nano Lett. **8**, 4229 (2008).

[31] E. H. Hwang and S. Das Sarma, Phys. Rev. B **77**, 115449 (2008).

[32] F. V. Tikhonenko, D. W. Horsell, R. V. Gorbachev, and A. K. Savchenko, Phys. Rev. Lett. **100**, 056802 (2008).

[33] J. Tworzydło, C. W. Groth, and C. W. J. Beenakker, Phys. Rev. B **78**, 235438 (2008).

[34] G. Borghi, M. Polini, R. Asgari, and A. H. MacDonald, Solid State Commun. **149**, 1117 (2009).

[35] J. Cserti, A. Csordás, and G. Dávid, Phys. Rev. Lett. **99**, 066802 (2007).

[36] A. S. Mayorov, D. C. Elias, M. Mucha-Kruczynski, R. V. Gorbachev, T. Tudorovskiy, A. Zhukov, S. V. Morozov, M. I. Katsnelson, V. I. Fal'ko, A. K. Geim, and K. S. Novoselov, Science **333**, 860 (2011).

[37] J. K. Viljas, A. Fay, M. Wiesner, and P. J. Hakonen, Phys. Rev. B **83**, 205421 (2011).

[38] A. Fay, R. Danneau, J. K. Viljas, F. Wu, M. Y. Tomi, J. Wengler, M. Wiesner, and P. J. Hakonen, Phys. Rev. B **84**, 245427 (2011).

[39] D. F. Santavicca, J. D. Chudow, D. E. Prober, M. S. Purewal, and P. Kim, Nano Lett. **10**, 4538 (2010).

[40] Y. M. Blanter and M. Büttiker, Phys. Rep. **336**, 1 (2000).

[41] R. Danneau, F. Wu, M. F. Craciun, S. Russo, M. Y. Tomi, J. Salmilehto, A. F. Morpurgo, and P. J. Hakonen, J. Low Temp. Phys. **153**, 374 (2008).

[42] M. Oksanen, A. Uppstu, A. Laitinen, D. J. Cox, M. F. Craciun, S. Russo, A. Harju, and P. Hakonen, Phys. Rev. B **89**, 121414 (2014).

[43] A. Laitinen, S. Paraoanu, M. Oksanen, M. F. Craciun, S. Russo, E. Sonin, and P. Hakonen, arXiv:1502.04330 (2015).

[44] According to the electrostatic contact analysis of Ref. [42], applicable also for a bilayer, the contact capacitance amounts to $C_c = 9.8 \times 10^{-6}\mathrm{F/cm}^2$ for Au/Cr/Au contacts similar to ours. Hence, we may estimate the real part $R_c$ of the impedance at the contact; $R$ in parallel with contact capacitance $C : R_c = R/[1 + (\omega C R)^2]$. Using the above value for $C_c$ and a contact area of 4 $\mu\mathrm{m}^2$, we obtain $(\omega C R)^2 \sim 10$ at $\omega/2\pi \sim 1$ GHz, which yields about 100 Ω instead of 1 kΩ for the high-frequency contact resistance.